Radiation Effects & Defects in Solids, 2013
Vol. 168, Nos. 11–12, 1011–1021, http://dx.doi.org/10.1080/10420150.2013.811504

Taylor & Francis
Taylor & Francis Group

A new interactive thermoluminescence mixed-order glow curve deconvolution function

M. Zahedifar* and S. Harooni

TL Lab, Department of Physics, University of Kashan, Kashan, Islamic Republic of Iran

(*Received 19 January 2013; final version received 20 May 2013*)

An interactive mixed-order thermoluminescence (TL) glow curve deconvolution function is presented for the first time in which the retrapping of thermally stimulated charge carriers in deep traps during the heating stage is taken into account. Considering this transition in the set of differential equations by describing the TL process and by solving them, an analytical function for TL intensity was obtained. This equation reduces to the known deconvolution function for the mixed-order model in the limiting case of saturation of deep trapping (DT) states. In intermediate cases, where the DT states are partially occupied, the proposed function acts as a real interactive model which allows the thermally stimulated electrons to be retrapped to deep electron traps. Applicability of the proposed model in a real TL system is also presented and discussed.

Keywords: thermoluminescence; interactive; mixed-order model; deep traps

1. Introduction

Different models have been presented for describing thermoluminescence (TL) of solids. The first-order kinetics of Randall and Wilkins (*1*) and second-order kinetics of Garlik and Gibson (*2*) are amongst the basic TL models. However, there are many experimental glow peaks with shapes that are not in accordance with first or second orders of kinetics. In order to study the intermediate cases, where the kinetic order is not necessarily one or two, May and Partridge presented the general-order (GO) model of kinetics as following (*3*):

$$I(T) = n_0 s \exp\left(-\frac{E}{kT}\right)\left(1 + (b-1)\frac{s}{\beta}\int_{T_0}^{T} \exp\left(-\frac{E}{kT'}\right) \mathrm{d}T'\right)^{-b/(b-1)}, \tag{1}$$

where I ($\mathrm{cm}^{-3}\ \mathrm{s}^{-1}$) is the TL intensity, n_0 (cm^{-3}) is the initial concentration of carriers in traps, s (s^{-1}) is the frequency factor, E (eV) is the activation energy, k (eV/K) is Boltzman's constant, T (K) is the sample temperature, β ($\mathrm{K\,s}^{-1}$) is the heating rate, and b is the order of kinetics which takes values between one and two and somewhat beyond this range. Despite of extensive investigations on improving the GO model and using it to estimate the kinetic parameters of TL phosphors (*4–7*), it cannot be derived directly from a set of equations governing the traffic of charge carries between trapping states, conduction band, and recombination centers (RCs) (*8*) and the parameter b could not be assigned an exact physical implication. Looking at the practical

*Corresponding author. Email: zhdfr@kashanu.ac.ir

side, the mixed-order (MO) kinetics model has a clear physical explanation, e.g. all parameters used in the model are not disputable from the physical point of view. It is more suitable to use this model for physical analysis of TL process, because the obtained results could be directly assigned with real parameters defining the process (*9*, *10*). The function describing the MO model is more complex than that of GO model (*8*, *9*):

$$I(T) = \frac{c^2 s' \alpha \exp(-E/kT) \exp((cs'/\beta) \int_{T_0}^{T} \exp(-E/kT')\, \mathrm{d}T')}{\{\exp((cs'/\beta) \int_{T_0}^{T} \exp(-E/kT')\, \mathrm{d}T') - \alpha\}^2}, \tag{2}$$

where $\alpha = n_0/(n_0 + c)$ and $s' = s/(N + c)$. c (cm^{-3}) is the concentration of electrons in thermally disconnected deep traps (TDDTs), N (cm^{-3}) is the concentration of trapping states, and the other parameters are as defined in Equation (1). It is shown that for $c \gg n_0$ ($\alpha \approx 0$), Equation (2) reduces to the first-order model and for $c = n_0$ ($\alpha \approx 1$) it approaches to the second-order model (*8*, *9*). So, the MO model includes not only the first and second orders of kinetics, but also the intermediate cases. It is important to note that obtaining the parameter α from an experimental TL peak leads one to know the physically meaningful parameter c, while it cannot be drawn any meaningful information from the value of the parameter b. The applicability of the GO and MO models in real TL glow peaks have been extensively investigated. Results of studies on kinetic analysis of the main dosimetry glow peaks of two well-known phosphors of LiF:Mg,Ti (TLD-100) and LiF:Mg,Cu,P (GR-200) have shown that the MO model has advantage over GO model (*11*, *12*). According to the MO model, there is one type of active trap (AT) and one type of RC in addition to TDDTs. The advantage of MO model is that it takes into account (via parameter c) the concentration of trapped electrons or holes in TDDTs during irradiating the sample. These charge carries do not take part in TL process in the considered temperature range due to being in deep traps or in low probability RCs. The main disadvantage of the MO model is that the TDDTs are non-interactive, i.e. they do not capture the electrons excited to conduction band from the ATs during the TL readout. In other words, it is implicit in MO model that the deep traps are saturated and as a result, the concentration of electrons in these traps remains constant during the TL emission (*13*, *14*). This is evidently not a practical assumption. The electrons thermally stimulated to the conduction band during heating the sample are likely to be retrapped in ATs as well as in TDDTs. Only when the deep traps are saturated, the retrapping to these sites is not allowed. In this work, the MO model is improved by allowing the thermally stimulated electrons to be retrapped in deep traps during the TL process and an analytical function is derived for the TL intensity which simply reduces to the common MO model in the limiting case, where the deep traps are saturated. In the intermediate cases, where the deep traps are partially occupied, the proposed model, as is expected, predicts the concentration of electrons in deep traps to increase during the heating stage.

2. Proposed function for IMO model

The level scheme for the proposed model of one AT, one RC, and deep trapping (DT) state is shown in Figure 1, where A_m ($\mathrm{cm}^3\ \mathrm{s}^{-1}$) is the recombination probability, A_n ($\mathrm{cm}^3\ \mathrm{s}^{-1}$) is the retrapping probability for ATs, and A_c ($\mathrm{cm}^3\ \mathrm{s}^{-1}$) is the retrapping probability for deep traps. The set of three following simultaneous differential equations describe the traffic of charged carriers during the heating stage:

$$-\frac{\mathrm{d}n}{\mathrm{d}t} = ns \exp\left(-\frac{E}{kT}\right) - A_n(N - n)n_c, \tag{3}$$

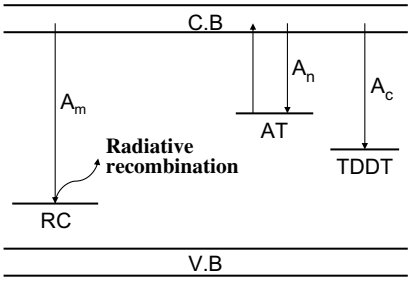

Figure 1. Schematic energy levels diagram for the proposed IMO model.

$$\frac{\mathrm{d}c}{\mathrm{d}t} = (H - c)A_c n_c, \tag{4}$$

$$m = n + c + n_c \rightarrow \frac{\mathrm{d}m}{\mathrm{d}t} = \frac{\mathrm{d}n}{\mathrm{d}t} + \frac{\mathrm{d}c}{\mathrm{d}t} + \frac{\mathrm{d}n_c}{\mathrm{d}t}, \tag{5}$$

$$I(t) = -\frac{\mathrm{d}m}{\mathrm{d}t} = A_m m n_c. \tag{6}$$

In the above equations, n_c (cm^{-3}) is the concentration of electrons in conduction band, n (cm^{-3}) is the concentration of electrons in ATs, c (cm^{-3}) is the concentration of electrons in deep traps, m (cm^{-3}) is the concentration of holes in centers, and H (cm^{-3}) is the total number of available states in deep traps. S (s^{-1}), E (eV), k ($\mathrm{eV\,K}^{-1}$), T (K), and N (cm^{-3}) are the same as in Equations (1) and (2). Equation (3) of the above set of differential equations describes the variation of concentration of electrons in ATs and the newly entered Equation (4) explains the rate of filling of deep traps via retrapping of thermally stimulated electrons. The retrapping of the excited electrons in deep electron traps has not been considered in MO model, since in this model, the deep traps are assumed to be filled ($c_0 = \mathrm{H}$) and thus, the electrons cannot be trapped in these sites during the TL process. The advantage of the proposed interactive mixed-order (IMO) model is that the electrons excited to conduction band are allowed to be retrapped in deep electron traps. This transition is explained in Equation (4) in which c, the concentration of electrons in deep traps is assumed to vary during the heating stage.

The most important assumption introduced into the present IMO model and the MO model is that of quasi-equilibrium approximation $|\mathrm{d}n_c/\mathrm{d}t| \ll |\mathrm{d}n/\mathrm{d}t|$ and $|\mathrm{d}n_c/\mathrm{d}t| \ll |\mathrm{d}c/\mathrm{d}t|$ (*15*). This assumption is of crucial importance and states that the concentration of electrons in the conduction band is quasi-stationary. The above inequalities are combined with the additional assumption that the initial concentration of carriers in the conduction band is small, which means that the free charge carriers never accumulate in the conduction band. Thus, the rate Equations (3)–(6) result in the following equation for n_c:

$$n_c = \frac{ns\exp(-E/kT)}{A_m m + A_n(N - n) + A_c(H - c)}. \tag{7}$$

Applying the condition $A_m = A_n = A_c$ in Equation (7) results in:

$$n_c = \frac{ns\exp(-E/kT)}{A_n(N + H + m - n - c)}. \tag{8}$$

It is worth noting that in deriving the analytical function for the TL intensity in the MO model (Equation (2)), the parameters A_m and A_n have been assumed to be the same. These parameters, A_m and A_n, can be defined as the product of the cross section for the recombination (trapping) and

the thermal velocity of the free carriers, $A_n = \sigma_n \cdot \upsilon$, where σ_n is the cross section (cm^2) and υ is the thermal velocity of the free electrons in the conduction band ($cm\ s^{-1}$). Despite the temperature dependence of A_m and A_n via parameter υ, these factors are assumed to remain unchanged in the temperature range of the corresponding TL glow peak (*9*, *16*). In the present IMO model, as is evident in Equation (11), the parameter A_n does not appear in the final expression for the TL intensity by replacing n_c from Equation (10) to Equation (3). Neglecting n_c in comparison with n and c in Equation (5) gains:

$$m = n + c. \tag{9}$$

Replacing this value for m in Equation (8) results in:

$$n_c = \frac{ns\exp(-E/kT)}{A_n(N+H)}. \tag{10}$$

Inserting the above function for n_c in Equation (3) gives the following:

$$-\frac{\mathrm{d}n}{\mathrm{d}t} = ns\exp\left(-\frac{E}{kT}\right) - (N-n)\frac{ns\exp(-E/kT)}{(N+H)}. \tag{11}$$

The time dependency in the above equation is changed to temperature dependency by using $T = T_0 + \beta t$ and $\mathrm{d}n/\mathrm{d}t = \mathrm{d}n/\mathrm{d}T \times \mathrm{d}T/\mathrm{d}t$, where β ($K\ s^{-1}$) is the heating rate and T_0 (K) is the initial temperature:

$$-\beta\frac{\mathrm{d}n}{\mathrm{d}T} = n(n+H)s'\exp\left(-\frac{E}{kT}\right). \tag{12}$$

In the above equation, the parameter s' is introduced as $s' = s/(N+H)$. Solving this differential equation for obtaining n as a function of T results in:

$$n(T) = \frac{n_0 H}{[(n_0+H)\exp((Hs'/\beta)\int_{T_0}^{T}\exp(-E/kT')\,\mathrm{d}T') - n_0]}. \tag{13}$$

Inserting Equation (10) into Equation (6) and using $T = T_0 + \beta t$ gives:

$$-\beta\frac{\mathrm{d}m}{\mathrm{d}T} = mns'\exp\left(-\frac{E}{kT}\right) \tag{14}$$

By inserting the value of n from Equation (13) to Equation (14) and by solving it for $m(T)$ obtains:

$$m(T) = \frac{m_0 H}{[(n_0+H) - n_0\exp(-(Hs'/\beta)\int_{T_0}^{T}\exp(-E/kT')\,\mathrm{d}T')]}. \tag{15}$$

Substituting Equation (15) in Equation (6) and noting $T = T_0 + \beta t$ acquires:

$$I(T) = m_0 n_0 \frac{H^2}{(n_0+H)^2}s'\exp\left(-\frac{E}{kT}\right)\frac{\exp((Hs'/\beta)\int_{T_0}^{T}\exp(-E/kT')\,\mathrm{d}T')}{[\exp((Hs'/\beta)\int_{T_0}^{T}\exp(-E/kT')\,\mathrm{d}T') - n_0/(n_0+H)]^2}. \tag{16}$$

By considering $m_0 = n_0 + c_0$ and introducing $\alpha = n_0/(n_0+H)$, the final equation for the proposed IMO model results in:

$$I(T) = H^2\alpha^2\frac{n_0+c_0}{n_0}s'\exp\left(-\frac{E}{kT}\right)\frac{\exp((Hs'/\beta)\int_{T_0}^{T}\exp(-E/kT')\,\mathrm{d}T')}{[\exp((Hs'/\beta)\int_{T_0}^{T}\exp(-E/kT')\,\mathrm{d}T') - \alpha]^2}. \tag{17}$$

It is worth noting that for $c_0 = H$, the above equation reduces to Equation (2).

3. Results

The correspondence of the proposed IMO model and MO model for the limiting case of $c_0 = H$ is shown in Figure 2. In this figure, the hollow circles are related to the glow peak generated by using MO model and the prolonged lines are pertinent to the glow peak plotted by using the function for TL intensity of IMO model (Equation (17)). The parameters used for generating this figure are $n_0 = 9 \times 10^{13}$ (cm^{-3}), $N = 1 \times 10^{14}$ (cm^{-3}), $s = 1 \times 10^{12}$ (s^{-1}), $E = 1$ (eV), and $\beta = 1$ (K s^{-1}). Higher (lower) heating rates cause both the generated and fitted glow peaks to shift to higher (lower) temperatures. The obtained results on superiority of the IMO model should not be affected by using different values of heating rates. It is evident in this figure that in the limiting case of $c_0 = H$ which corresponds to saturation of deep electron traps, the glow peaks generated by using IMO model are entirely coincide to those of MO model. In Figure 3, the TL glow peaks are plotted using Equation (17) with $\alpha = 0.5, n_0 = 9 \times 10^{13}$ (cm^{-3}), $N = 1 \times 10^{14}$ (cm^{-3}), $s = 1 \times 10^{12}$ (s^{-1}), $E = 1$ (eV), and $\beta = 1$ (K s^{-1}) and different values for the initial populations of deep electron traps, c_0. As is observed, with decrease in parameter c_0, the glow peak area decreases due to an increase in retrapping of thermally excited electrons in deep traps. This effect was observed experimentally and will be discussed in this section. To compare the TL glow peaks produced by using the IMO model (Equation (17)) with those of MO model (Equation (2)), a set of 36 glow peaks of IMO with different values of α (the parameter which governs the symmetry of glow peaks) and c_0/H (the fraction of initial population of deep traps) were generated as given in Table 1. The line numbers (L.ns) 1–9 correspond to $c_0/H = 1$ (which describe the saturation of deep traps) and different values of α from 0.1–1. Four groups are given in Table 1, each with the same parameter c_0/H and different values of α. In the last group, the parameter c_0/H is 0.1 which demonstrates minimum initial population of deep traps. Other parameters used to produce 36 glow peaks of IMO model are $n_0 = 9 \times 10^{13}$ (cm^{-3}), $N = 1 \times 10^{14}$ (cm^{-3}), $s = 1 \times 10^{12}$ (s^{-1}), $E = 1$ (eV), and $\beta = 1$ (K s^{-1}). Then, the glow curve deconvolution function of MO model (Equation (2)) was fitted to all the generated IMO glow peaks of Table 1. A computer program developed in our laboratory using Levenberg–Margart algorithm based on non-linear least square method was used to fit the MO glow curve deconvolution function (Equation (2)) to the generated

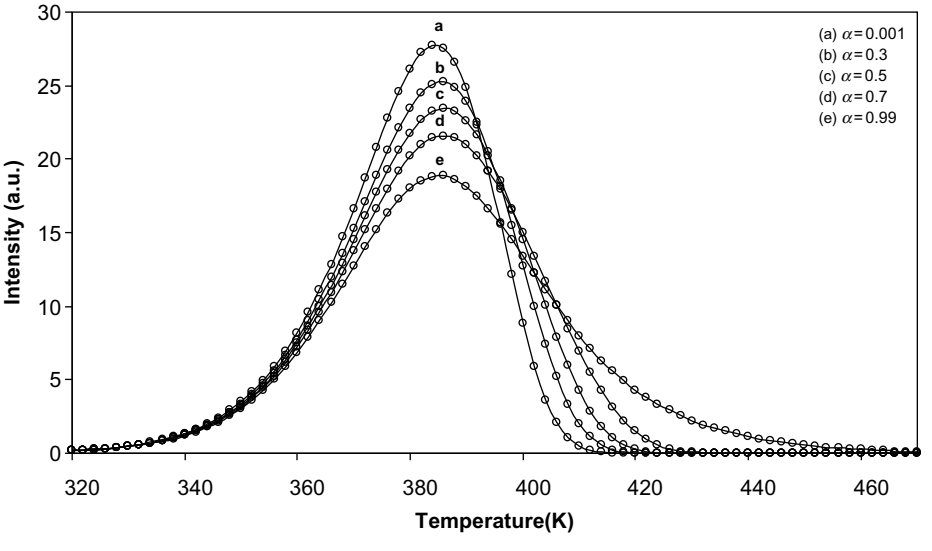

Figure 2. TL glow peaks generated by using the MO model (open circles) and the IMO model (solid curves) for the limiting case of saturation of deep traps and different values of the parameter α.

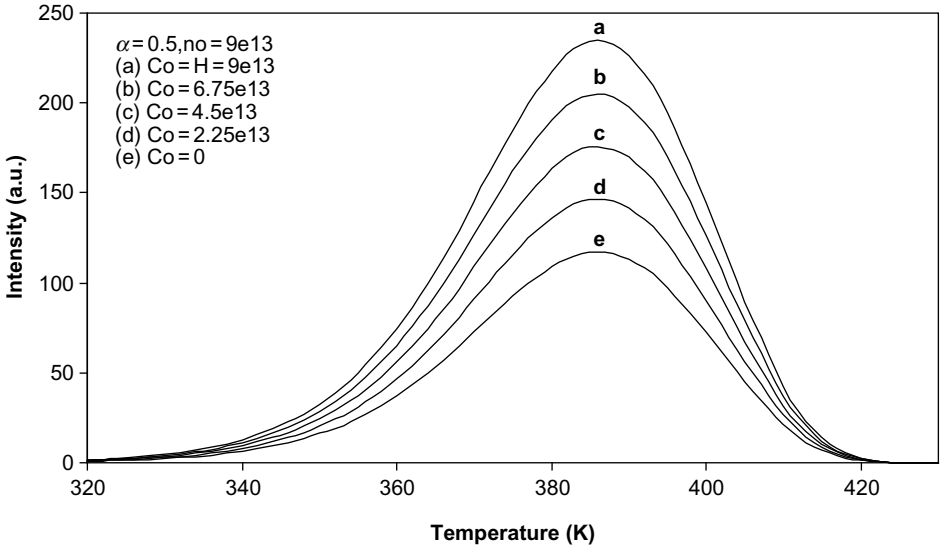

Figure 3. TL glow peaks of IMO model with different initial populations of DT states c_0. $\alpha = 0.5$ and $n_0 = 9 \times 10^{13}$ (cm^{-3}) for all produced glow peaks.

Table 1. Thirty-six pairs of parameters α and c_0/H used to generate the glow peaks of IMO expression (Equation (17)).

	Parameters			Parameters	
L.N.	α	$c_{o/H}$	L.N.	α	$c_{o/H}$
1	0.10	1.0	19	0.10	0.3
2	0.20	1.0	20	0.20	0.3
3	0.30	1.0	21	0.30	0.3
4	0.40	1.0	22	0.40	0.3
5	0.50	1.0	23	0.50	0.3
6	0.60	1.0	24	0.60	0.3
7	0.70	1.0	25	0.70	0.3
8	0.80	1.0	26	0.80	0.3
9	0.99	1.0	27	0.99	0.3
10	0.10	0.6	28	0.10	0.1
11	0.20	0.6	29	0.20	0.1
12	0.30	0.6	30	0.30	0.1
13	0.40	0.6	31	0.40	0.1
14	0.50	0.6	32	0.50	0.1
15	0.60	0.6	33	0.60	0.1
16	0.70	0.6	34	0.70	0.1
17	0.80	0.6	35	0.80	0.1
18	0.99	0.6	36	0.99	0.1

Notes: In each nine consecutive lines, the parameter c_0/H remains unchanged, while the parameter α varies from 0.1 to 0.99. Other parameters are $n_0 = 9 \times 10^{13}$ (cm^{-3}), $N = 1 \times 10^{14}$ (cm^{-3}), $s = 1 \times 10^{12}$ (s^{-1}), $E = 1$ (eV), and $\beta = 1$ ($K\,s^{-1}$).

IMO glow peaks of Table 1. For testing the goodness of fit, the figure of merit (FOM) was used (*17*):

$$\mathrm{FOM} = \sum_{j_f}^{j_l} \frac{100[y_i - y(x_i)]}{A}, \tag{18}$$

where j_f and j_l are the numbers of the first and last temperature interval ΔT used for curve fitting, Y_i is the intensity in the ith interval obtained from the experiment, $Y(x_i)$ is the intensity expected from the model, and A is the total area of fitted glow peak between j_f and j_l. The FOM values lower than 2.5% show a good fitness to the experimental glow curves.

In order to further reveal the difference between the two models, the MO model (Equation (2)) was fitted to the 36 glow peaks of Table 1; while the parameters, H (concentration of DT states), N (concentration of dosimetry trapping states), and n_0 (initial population of dosimetry traps), of MO model were kept to be the same as those of IMO model of Table 1. Consequently, the kinetic parameters E (activation energy) and s (frequency factor) were considered as free parameters during fitting of Equation (2) to the 36 generated IMO glow peaks of Table 1. As it is observed, the low FOM values are obtained only for L.ns 1–9 where the condition $c_0/H = 1$ is fulfilled. Going far from saturation, which corresponds to reduction of the fraction c_0/H, causes the fitted values for E and s to differ from the corresponding parameters of Table 1 and the FOM value to

Table 2. Kinetic parameters of MO model obtained by fitting Equation (2) to the synthetic IMO glow peaks of Table 1.

	Kinetic parameters of the MO model obtained by fitting Equation (2) to IMO glow peaks of Table 1 with the same values of N and n_0					
L.N.	α	N (cm^{-3})	n_0 (cm^{-3})	s (s^{-1})	E (eV)	FOM (%)
1	0.10	1.000×10^{14}	9.000×10^{13}	1.000×10^{12}	1.000	0
2	0.20	1.000×10^{14}	9.000×10^{13}	1.000×10^{12}	1.000	0
3	0.30	1.000×10^{14}	9.000×10^{13}	1.000×10^{12}	1.000	0
4	0.40	1.000×10^{14}	9.000×10^{13}	1.000×10^{12}	1.000	0
5	0.50	1.000×10^{14}	9.000×10^{13}	1.000×10^{12}	1.000	0
6	0.60	1.000×10^{14}	9.000×10^{13}	1.000×10^{12}	1.000	0
7	0.70	1.000×10^{14}	9.000×10^{13}	1.000×10^{12}	1.000	0
8	0.80	1.000×10^{14}	9.000×10^{13}	1.000×10^{12}	1.000	0
9	0.99	1.000×10^{14}	9.000×10^{13}	1.000×10^{12}	1.000	0
10	0.10	1.000×10^{14}	9.000×10^{13}	4.519×10^{07}	0.678	8.19
11	0.20	1.000×10^{14}	9.000×10^{13}	1.914×10^{08}	0.724	16.16
12	0.30	1.000×10^{14}	9.000×10^{13}	7.331×10^{08}	0.767	14.14
13	0.40	1.000×10^{14}	9.000×10^{13}	2.556×10^{09}	0.807	12.11
14	0.50	1.000×10^{14}	9.000×10^{13}	8.154×10^{09}	0.844	10.09
15	0.60	1.000×10^{14}	9.000×10^{13}	2.389×10^{10}	0.879	8.073
16	0.70	1.000×10^{14}	9.000×10^{13}	6.457×10^{10}	0.911	6.054
17	0.80	1.000×10^{14}	9.000×10^{13}	1.627×10^{11}	0.941	4.036
18	0.99	1.000×10^{14}	9.000×10^{13}	9.054×10^{11}	0.997	0.202
19	0.10	1.000×10^{14}	9.000×10^{13}	1.229×10^{04}	0.421	31.79
20	0.20	1.000×10^{14}	9.000×10^{13}	2.439×10^{04}	0.441	28.32
21	0.30	1.000×10^{14}	9.000×10^{13}	2.869×10^{05}	0.518	24.78
22	0.40	1.000×10^{14}	9.000×10^{13}	5.915×10^{06}	0.613	21.23
23	0.50	1.000×10^{14}	9.000×10^{13}	8.371×10^{07}	0.697	17.68
24	0.60	1.000×10^{14}	9.000×10^{13}	8.359×10^{08}	0.771	14.14
25	0.70	1.000×10^{14}	9.000×10^{13}	6.265×10^{09}	0.836	10.60
26	0.80	1.000×10^{14}	9.000×10^{13}	3.729×10^{10}	0.894	7.066
27	0.99	1.000×10^{14}	9.000×10^{13}	8.401×10^{11}	0.994	0.354
28	0.10	1.000×10^{14}	9.000×10^{13}	8.746×10^{03}	0.414	40.70
29	0.20	1.000×10^{14}	9.000×10^{13}	9.522×10^{03}	0.415	36.26
30	0.30	1.000×10^{14}	9.000×10^{13}	1.113×10^{04}	0.417	31.81
31	0.40	1.000×10^{14}	9.000×10^{13}	4.072×10^{04}	0.457	27.32
32	0.50	1.000×10^{14}	9.000×10^{13}	1.795×10^{06}	0.575	22.76
33	0.60	1.000×10^{14}	9.000×10^{13}	6.021×10^{07}	0.687	18.19
34	0.70	1.000×10^{14}	9.000×10^{13}	1.109×10^{09}	0.780	13.63
35	0.80	1.000×10^{14}	9.000×10^{13}	1.311×10^{10}	0.860	9.087
36	0.99	1.000×10^{14}	9.000×10^{13}	7.992×10^{11}	0.993	0.455

Notes: The parameters H, N, and n_0 were kept the same as those of Table 1. As is observed, the low FOM values are correspond only to saturation of deep traps, where $c_0/H = 1$.

increase. It is worth noting that the MO model predicts that all the electrons thermally excited to conduction band during the TL process undergo radiative recombination, that is the excited electrons are not loosed by retrapping in deep traps since these traps are non-interactive during the TL process. In IMO model, however, the deep traps are non-interactive during the TL process only when the saturation condition is governed. By going far from saturation, a fraction of thermally stimulated electrons do not contribute in TL by being retrapped in deep electron traps. During fitting of MO model to the generated IMO glow peaks of Table 1, the initial population of dosimetry traps n_0, the available states in these traps N, and the available states in deep traps H are considered to be the same. Thus, the two models produce the same glow peaks when all thermally stimulated electrons undergo radiative recombination (L.ns 1–9 of Table 2). By going far from saturation of deep traps ($c_0/H < 1$), the IMO model predicts that a fraction of n_0 (initial population of electrons in dosimetry traps) do not contribute in TL; while according to the MO model, all the n_0 populated electrons in dosimetry traps undergo radiative recombination. Therefore, the MO

Table 3. Results obtained by fitting the MO model to the synthetic IMO glow peaks of Table 1.

	Kinetic parameters obtained by fitting the MO model to 36 IMO glow peaks of Table 1. All parameters are free to change during the fitting process					
L.N.	α	N (cm^{-3})	n_0 (cm^{-3})	s (s^{-1})	E (eV)	FOM (%)
1	0.10	1.000×10^{14}	9.000×10^{13}	1.000×10^{12}	1	0
2	0.20	1.000×10^{14}	9.000×10^{13}	1.000×10^{12}	1	0
3	0.30	1.000×10^{14}	9.000×10^{13}	1.000×10^{12}	1	0
4	0.40	1.000×10^{14}	9.000×10^{13}	1.000×10^{12}	1	0
5	0.50	1.000×10^{14}	9.000×10^{13}	1.000×10^{12}	1	0
6	0.60	1.000×10^{14}	9.000×10^{13}	1.000×10^{12}	1	0
7	0.70	1.000×10^{14}	9.000×10^{13}	1.000×10^{12}	1	0
8	0.80	1.000×10^{14}	9.000×10^{13}	1.000×10^{12}	1	0
9	0.99	1.000×10^{14}	9.000×10^{13}	1.000×10^{12}	1	0
10	0.10	1.005×10^{14}	5.760×10^{13}	1.063×10^{12}	1	0
11	0.20	9.823×10^{13}	6.120×10^{13}	1.097×10^{12}	1	0
12	0.30	9.630×10^{13}	6.480×10^{13}	1.109×10^{12}	1	0
13	0.40	9.507×10^{13}	6.840×10^{13}	1.107×10^{12}	1	0
14	0.50	9.458×10^{13}	7.200×10^{13}	1.096×10^{12}	1	0
15	0.60	9.475×10^{13}	7.560×10^{13}	1.080×10^{12}	1	0
16	0.70	9.546×10^{13}	7.920×10^{13}	1.061×10^{12}	1	0
17	0.80	9.662×10^{13}	8.280×10^{13}	1.041×10^{12}	1	0
18	0.99	9.980×10^{13}	8.964×10^{13}	1.002×10^{12}	1	1×10^{-6}
19	0.10	9.584×10^{13}	3.330×10^{13}	1.175×10^{12}	1	0
20	0.20	9.060×10^{13}	3.960×10^{13}	1.230×10^{12}	1	0
21	0.30	8.778×10^{13}	4.590×10^{13}	1.233×10^{12}	1	0
22	0.40	8.692×10^{13}	5.220×10^{13}	1.212×10^{12}	1	0
23	0.50	8.745×10^{13}	5.850×10^{13}	1.182×10^{12}	1	0
24	0.60	8.891×10^{13}	6.480×10^{13}	1.147×10^{12}	1	0
25	0.70	9.105×10^{13}	7.110×10^{13}	1.110×10^{12}	1	0
26	0.80	9.377×10^{13}	7.740×10^{13}	1.074×10^{12}	1	0
27	0.99	1.007×10^{14}	8.937×10^{13}	1.014×10^{12}	1	1×10^{-6}
28	0.10	8.289×10^{13}	1.710×10^{13}	1.369×10^{12}	1	0
29	0.20	7.753×10^{13}	2.520×10^{13}	1.384×10^{12}	1	0
30	0.30	7.702×10^{13}	3.330×10^{13}	1.349×10^{12}	1	0
31	0.40	7.748×10^{13}	4.140×10^{13}	1.300×10^{12}	1	0
32	0.50	8.100×10^{13}	4.950×10^{13}	1.249×10^{12}	1	0
33	0.60	8.413×10^{13}	5.760×10^{13}	1.197×10^{12}	1	0
34	0.70	8.769×10^{13}	6.570×10^{13}	1.145×10^{12}	1	0
35	0.80	9.167×10^{13}	7.380×10^{13}	1.096×10^{12}	1	0
36	0.99	1.008×10^{14}	8.919×10^{13}	1.017×10^{12}	1	1×10^{-6}

Notes: The only difference compared to Table 2, is that all the kinetic parameters of the MO model are allowed to change during the fitting process. Despite the excellent conformity, the values obtained for n_0 and N of the MO model are different from those of the IMO model.

model fails to produce the same glow peak as the IMO model when the deep traps are partially occupied. The high FOM values and different fitted values for the activation energies and the frequency factors for L.ns 9–36 given in Table 2 can be explained in this way. In Table 3, the results of fitting of 36 generated glow peaks of Table 1 to the MO model are observed. The only difference between Tables 2 and 3 is that, in Table 3 all the kinetic parameters of the MO model were allowed to change during the fitting process. As is evident in Table 3, the obtained FOM values are near zero which confirms very good fits of MO glow peaks to the generated IMO glow peaks. However, only for L.ns. 1–9 the fitted values for n_0 and N are the same as those of IMO model. These L.ns correspond to saturation of deep traps. By going far from saturation, despite of good conformity of the MO and IMO glow peaks, the fitted MO glow peaks give values for n_0 and N which are different from the corresponding parameters of the generated IMO model. Precisely speaking, the MO model gives lower values for n_0 and N compared to the IMO model to compensate the fraction of charge carriers which are not allowed to be retrapped in deep electron states in MO model and to produce the best fit to the generated IMO glow peaks of Table 1. Taking into consideration that the IMO model is more physical than the Mo model, the obtained kinetic parameters using IMO model are more reliable than those of Mo model. Also, the proposed IMO model was tested in a real TL system. For doing so, the main glow peak of the well known $Al_2O_3 : C$(TLD-500) phosphor was selected for comparing the applicability of two models in a real system. The latest report reveals three component glow peaks for the TL glow curve of this phosphor (*18*). Therefore, the three components were incorporated in the curve-fitting procedure. The results are shown in Figures 4 and 5. All the TL measurements were performed with a TL reader model 4500 from Harshaw using a linear heating rate of 1°C/s. In Figure 4, the experimental glow curve of $Al_2O_3 : C$(TLD-500) is shown with hollow circles and the outcomes of fitting the experimental glow curve with IMO and MO are observed with triangles and crosses, respectively. Both the MO and IMO glow curves are seen to fit fairly to the experimental glow curve. This result is understood by considering the absorbed dose of 10 Gy which is near saturation dose for TLD-500 phosphor. As pointed out earlier, the MO model approaches to IMO model when deep traps are near saturation. However, the FOM values for the fitted glow curves for the absorbed dose of 7 Gy differ considerably as is shown in Figure 5. This behavior is explained based on the different initial populations of deep traps shown in Figures 4 and 5. For higher absorbed doses, the population of deep traps approaches to saturation and thus, both the MO and IMO models can describe the system properly. However, for far from saturation of deep traps, the IMO model

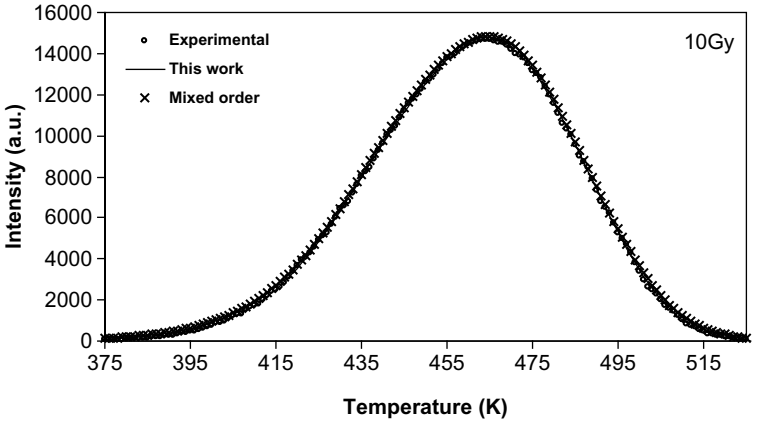

Figure 4. Experimental TL glow peaks of TLD-500 (open circles) fitted to the IMO (solid curve) and MO models (crosses) for the absorbed dose of 10 Gy.

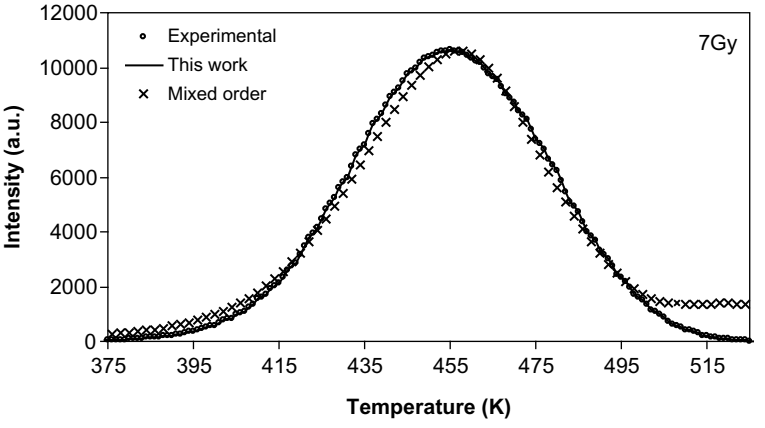

Figure 5. TL glow peaks of TLD-500 (Open circles) fitted to the IMO model (solid curve) and the MO model (crosses) for the absorbed dose of 7 Gy.

describes the system correctly, while the MO model fails to coincide to the experimental glow curve.

4. Conclusions

The main assumption of MO model is that $c = H$, i.e. the DT states are completely occupied. The proposed IMO glow curve deconvolution function is more physical, since it predicts via Equation (4) that a fraction of thermally stimulated electrons undergo retrapping in deep traps during the TL process. The comparison of MO and IMO models was carried out by fitting Equations (2) and (17) to the TL glow curves of TLD-500 recorded after irradiating the phosphor to different gamma doses. For saturation dose, where $c_0 = H$, the MO and IMO models are fitted fairly to the experimental glow curve. However, far from saturation, when the deep traps are partially occupied, ($c_0 \neq H$) the IMO model results in better conformity with the experimental glow curve and lower FOM value is obtained. Despite the assumption of $A_m = A_n = A_c$ is a restricting condition, (as the condition is $A_n = A_m$ for the MO model), however, the proposed model is more general and physical than the MO model.

Acknowledgements

The research council of the University of Kashan is gratefully acknowledged for its support of this work.

References

(1) Randall, J.T.; Wilkins, M.H.F. *Proc. Roy. Soc*. **1945,** *184,* 366–389.
(2) Garlick, G.F.J.; Gibson, A.F. *Proc. Phys. Soc.* **1948,** *60,* 574–589.
(3) May, C.E.; Partridge, J.A. *J. Chem. Phys.* **1964,** *40,* 1401–1415.
(4) Flores-Llamas, H.; Gutiérrez-Tapia, C. *Radiat. Eff. Def. Solids* **2013,** *168,* 48–60.
(5) Rasheedy, M.S. *Radiat. Eff. Def. Solids.* **2005,** *160,* 383–390.
(6) Sunta, C.M.; Mol, A.W.; Kulkarni, R.N.; Piters, T.M.; Chubaci, J.F.D.; Avta, W.E.F.; Watanabe, S. *Rad. Eff. Def. Solids* **1998,** *146,* 229–235.
(7) Song, K.W.; Kim, K.B.; Hong, D.G. *Radiat. Eff. Def. Solids* **2010,** *165,* 305–312.
(8) Chen, R.; Mckeever, S.W.S. *Theory of thermoluminescence and Related Phenomena*; World Scientific: Singapore, 1997.
(9) Chen, R.; Kristianpoller, N.; Davidson, Z.; Visocekas, R. *J. Lumin*. **1981,** *23,* 293–303.

(10) Kitis, G.; Chen, R.; Pagonis, V. *Phys. Status Solidi A* **2008,** *205,* 1181–1189.
(11) Yossian, D.; Horowitz, Y.S. *Radiat. Meas*. **1997,** *27,* 465–471.
(12) Zahedifar, M.; Kavianinia, M.J.; Ahmadi, M. *Radiat. Meas*. **2007,** *42,* 815–818.
(13) Maghrabi, M.; Al-Jundi, J.; Arafah, D.E. *Radiat. Prot. Dosim*. **2008,** *130,* 291–299.
(14) Sunta, C.M.; Ayta, W.E.F.; Chubaci, J.F.D.; Watanabe, S. *Radiat. Meas*. **2002,** *35,* 595–602.
(15) Gomez-Rose, J.M.; Furetta, C.; Correcher, V. *Radiat. Prot. Dosim*. **2006,** *119,* 339–343.
(16) Bos, A.J.J. *Radiat. Meas.* **2007,** *41,* S45–S56.
(17) Balian, H.G.; Eddy, N.W. *Nucl. Instrum. Methods* **1977,** *145,* 389–395.
(18) Zahedifar, M.; Eshraghi, E.; Sadeghi, E. *Radiat. Meas*. **2012,** *47,* 957–964.